ACS Catalysis

Research Article

pubs.acs.org/acscatalysis

# Synthesis of Na-Stabilized Nonporous t-$ZrO_2$ Supports and Pt/t-$ZrO_2$ Catalysts and Application to Water-Gas-Shift Reaction

Hong Xie,[†] Junling Lu,[‡] Mayank Shekhar,[§,∥] Jeffery W. Elam,[‡] W. Nicholas Delgass,[§] Fabio H. Ribeiro,[§] Eric Weitz,[†] and Kenneth R. Poeppelmeier*[,†]

[†]Center for Catalysis and Surface Science, Department of Chemistry, Northwestern University, 2145 Sheridan Road, Evanston, Illinois 60208, United States

[‡]Energy Systems Division, Argonne National Laboratory, 9700 South Cass Avenue, Argonne, Illinois 60439, United States

[§]School of Chemical Engineering, Purdue University, 480 Stadium Mall Drive, West Lafayette, Indiana 47907, United States

**ABSTRACT:** t-$ZrO_2$, synthesized under hydrothermal treatment conditions at 150 °C for 20 h using NaOH as the mineralizer, was phase stable up to 600 °C in air. The t-$ZrO_2$ calcined at 600 °C (denoted as Z600) were nonporous spherical nanocrystallites with an average size of ∼12 nm and a surface area of ∼55 $m^2/g$, which exhibited hydrothermal stability in a wide range of pH environments from acidic to basic conditions at 200 °C for 20 h. Monodispersed platinum nanoparticles ∼1.5 ± 0.3 nm were obtained on the Z600 supported Pt/t-$ZrO_2$ catalyst by the Pt atomic layer deposition (ALD) method. Na ions were found to play a crucial role in the formation of the stable t-$ZrO_2$ by incorporating into the internal crystal structure of $ZrO_2$ during the hydrothermal synthesis. The rate of water-gas-shift (WGS) reaction per mole of surface Pt on the Pt/Z600 catalyst was about five times higher compared to the catalysts prepared on commercial nonporous $ZrO_2$. The incorporation of Na into the t-$ZrO_2$ structure had a synergistic effect: stabilizing $ZrO_2$ in the tetragonal phase and promoting the WGS reaction.

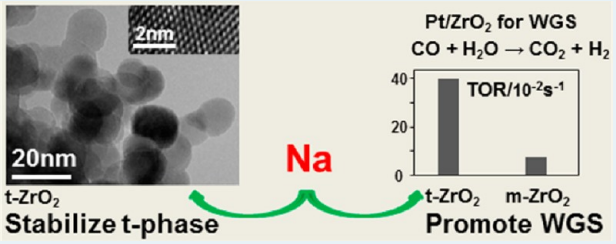


**KEYWORDS:** *tetragonal $ZrO_2$, hydrothermal synthesis, Na, Pt/$ZrO_2$, water-gas-shift reaction*

## 1. INTRODUCTION

$ZrO_2$ has been widely used as both a catalyst and a catalyst support material because of its high thermal stability and unique acidic and basic properties.[1] As a catalyst, $ZrO_2$ has been used to catalyze reactions including the dehydration of alcohols,[2,3] hydrogenation of CO[4−6] and olefins,[7] and isomerization of olefins.[8,9] As a catalyst support, $ZrO_2$ has been applied successfully for various reactions such as methanol synthesis,[6] steam reforming,[10] and epoxidation of olefins.[11] $ZrO_2$ exists primarily in three different polymorphs at ambient pressure: monoclinic (m-$ZrO_2$, room temperature-1175 °C), tetragonal (t-$ZrO_2$, 1175−2370 °C), and cubic (c-$ZrO_2$, 2370−2680 °C).[12] The crystal phases of $ZrO_2$ (monoclinic and tetragonal) can significantly affect the catalytic performance for chemical reactions. Ma et al. prepared t-$ZrO_2$ using $Na_2CO_3$ and reported that thus prepared t-$ZrO_2$ supported Cu catalyst showed the highest Cu dispersion and the best catalytic performance for methanol synthesis from CO hydrogenation compared to amorphous and m-$ZrO_2$.[6] Stichert reported that, for the sulfated zirconia catalysts, the t-$ZrO_2$ was about 4-fold more active than m-$ZrO_2$ for the n-butane isomerization reaction.[9] Chary et al. investigated the alkylation of phenol over $V_2O_5$ catalysts supported on m- and t-zirconia and found out that $V_2O_5$/m-$ZrO_2$ was 4-fold more active than $V_2O_5$/t-$ZrO_2$ for alkylation of phenol at 673 K.[13] These marked differences in catalytic performance for $ZrO_2$ render it necessary to synthesize pure phase $ZrO_2$. Compared to m-$ZrO_2$, t-$ZrO_2$ is thermodynamically metastable at low temperatures and will tend to transform to m-$ZrO_2$ upon thermal treatment or contact with water.[14] The preparation of low temperature stable t-$ZrO_2$, therefore, has been a challenge through the years. Various methods have been developed to synthesize stable tetragonal phase $ZrO_2$, including sol−gel,[15,16] precipitation,[6,13,14,17−19] and thermal decomposition methods.[15,20] However, most of these synthesis routes are complicated and need to use the relatively more expensive Zr alkoxide precursors, and result in the formation of irregularly shaped particles with a broad size distribution. Compared to these methods, hydrothermal synthesis has proved to have several advantages: it can be carried out at moderate temperatures around 100−300 °C; it can be used to synthesize materials of metastable phases, and it has been used to easily prepare nanosized powders with controlled sizes and shapes.[21,22] The t-$ZrO_2$ can be stabilized by introducing transition metal oxide compounds such as MgO and $Y_2O_3$.[23,24] However, the introduction of these metal oxide compounds may lead to unwanted reaction products or changes of reaction activities for catalytic reactions. Many factors have been considered to be responsible for the

**Received:** September 10, 2012
**Revised:** November 28, 2012
**Published:** December 4, 2012

   dx.doi.org/10.1021/cs300596q | *ACS Catal.* 2013, 3, 61−73

formation of metastable t-$ZrO_2$. For instance, the formation of metastable t-$ZrO_2$ at low temperature was correlated with a critical size,[15,20] the existence of amorphous $ZrO_2$,[25] and surface hydration structure.[21] The use of NaOH for $ZrO_2$ synthesis has been reported extensively. For instance, Garvie reported the use of 50 wt % NaOH for $ZrO_2$ synthesis using a precipitation method and concluded that the Na was a metal impurity and did not affect the formation of the different phases of the final $ZrO_2$ products.[20] Noh et al. reported the use of 5 M NaOH for synthesis of $ZrO_2$ which showed a faster t-m phase transformation compared to 1 M NaOH.[26] Wang et al. reported the use of 16 M NaOH for the synthesis of t-$ZrO_2$ with a size of less than 6 nm.[21] However, in these studies, the function of Na ions for the formation of t-$ZrO_2$ or m-$ZrO_2$ was not investigated systematically. So far, only a few studies of alkali metal effects on $ZrO_2$ phase formation have been reported.[16,18,19,27] The effect of Na on t-$ZrO_2$ formation has yet to be clarified.

Here, we report the preparation of t-$ZrO_2$ with controlled sizes via a combined hydrothermal-calcination method using an inexpensive and nontoxic inorganic compound of $ZrOCl_2{\cdot}8H_2O$ as the Zr precursor and NaOH as the mineralizer in the presence of organic additive aqueous solution. The t-$ZrO_2$ was first synthesized in an autoclave reactor by hydrothermal treatment with subsequent calcination at elevated temperatures. The Z600 t-$ZrO_2$ was used as catalyst support to prepare Pt/t-$ZrO_2$ catalysts by the ALD method. The WGS reaction was used as a model reaction to test the reaction activities of the Pt/t-$ZrO_2$ catalysts. The mechanism of the Na stabilization of the t-$ZrO_2$ and the Na promotion effect on the WGS reaction were investigated.

## 2. EXPERIMENTAL METHODS

**2.1. Preparation of $ZrO_2$ Support and Pt/$ZrO_2$ Catalyst.** *Materials.* $ZrOCl_2{\cdot}8H_2O$, $Pt(NH_3)_4(NO_3)_2$, and $NH_4OH$ (Sigma-Aldrich), absolute ethanol (Macron Chemicals), oleic acid (Alfa Aesar), NaOH (Fisher Scientific), Methylcyclopentadienyl-trimethyl platinum ($MeCpPtMe_3$, Strem Chemical), m-$ZrO_2$ (nonporous monoclinic $ZrO_2$, $S_{BET}$ = 24 $m^2/g$, Daiichi Kigenso Kagaku Kogyo Co., Ltd.), Zero air, UHP $N_2$, and $O_2$ (Airgas), $H_2$ (Praxair), CO (Indiana Oxygen), $CO_2$ (in house), and Ar (in house). All chemicals were used as received.

*2.1.1. Synthesis of $ZrO_2$.* $ZrO_2$ nanoparticles were synthesized via hydrothermal treatment by two approaches: in the absence and presence of organic additives. In the absence of organic additives, mineralizers including $NH_4OH$, KOH, and NaOH were used for the synthesis. Typically, 2 mmol $ZrOCl_2{\cdot}8H_2O$ was dissolved in DI water. Then designated amounts of mineralizers were added to the $ZrOCl_2$ aqueous solution. The total volume was adjusted to 40 mL using DI water when $NH_4OH$ was used, or 60 mL when KOH and NaOH were used. The reaction mixture was then transferred into a 125 mL autoclave Teflon liner, sealed, and heated at 150 °C for 10 h. In the presence of organic additives, 5 mmol $ZrOCl_2{\cdot}8H_2O$ was dissolved in 10 mL of DI water to yield a transparent clear solution. Then organic additives were added to generate white precipitates. Two different combinations of organic additives were adopted: 35 mL of absolute ethanol, or 5 mL of oleic acid dissolved in 35 mL of absolute ethanol. The reaction mixture was ultrasonicated for 1 h before adding 20 mL of 10 M NaOH, which led to a continuous viscosity increase of the mixture. After vigorous stirring for 30 min, the suspension mixture was transferred into a 125 mL Teflon-lined autoclave and heated at 150 °C for 20 h. In both approaches, the autoclaves were subsequently allowed to cool down to room temperature. The autoclave reaction mixture was then separated by centrifuge at 6500 rpm and washed exhaustively using absolute ethanol and DI water, and air-dried at 70 °C for 12 h. White powders were then collected and calcined in air at different temperatures from 300 to 800 °C for 3 h to form the final $ZrO_2$ products. The 70 °C air-dried t-$ZrO_2$ synthesized in the presence of organic additives was denoted as the as-synthesized t-$ZrO_2$.

*2.1.2. Pt/t-$ZrO_2$ Preparation.* Pt was deposited onto the Z600 t-$ZrO_2$ support by incipient wetness impregnation (IWI) and ALD. The 2% Pt/t-$ZrO_2$ sample was prepared by IWI with an aqueous solution of $Pt(NH_3)_4(NO_3)_2$ and $NH_4OH$. The sample was dried at 100 °C and calcined in flowing air at 225 °C for 3 h. ALD Pt was performed in a viscous flow stainless tube reactor system.[28] During the preparation, UHP $N_2$ carrier gas continuously passed through the tube reactor at a mass flow rate of 300 sccm and a pressure of 1 Torr. To maximize the Pt precursor utilization, a decreased pumping rate with a lower total $N_2$ flow of 200 sccm was adopted for the ALD Pt process. About 1.0 g of t-$ZrO_2$ support was loaded into the ALD reactor followed by a 10 min ozone treatment to remove possible surface carbonyls and additional 20 min to stabilize the ALD system at the deposition temperature. Then the ALD Pt process was conducted at 200 or 300 °C by sequential exposure of $MeCpPtMe_3$ for 300 s and $O_2$ for 200 s with 50 s $N_2$ purge in between. The $MeCpPtMe_3$ precursor was contained in a stainless steel bubbler and heated at 50 °C to produce a practical vapor pressure.[29] $N_2$ with a flow rate of 30 sccm passed through the bubbler and carried the $MeCpPtMe_3$ vapor phase precursor into the reaction chamber. The inlet lines were heated to at least 150 °C to prevent vapor phase condensation. The resulting catalyst from the ALD procedure was denoted as 3.9% Pt/t-$ZrO_2$. Two m-$ZrO_2$ supported catalysts of the 0.6% Pt/m-$ZrO_2$ and 5.9% Pt/m-$ZrO_2$ were also prepared by one Pt ALD cycle at deposition temperatures of 200 and 300 °C, respectively. Pt loadings were expressed in Pt wt %.

**2.2. Characterization.** *X-ray Powder Diffraction (XRD).* XRD patterns of the samples were recorded at room temperature on a Rigaku diffractometer (Cu−K radiation, Ni filter, 40 kV, 20 mA, $2\theta$ = 10−70°, 0.1° step size, and 2 s count time). The volume fraction, $V_t$, of t-$ZrO_2$ was determined using the following relationships:[30]

$$X_m = \frac{I_m(111) + I_m(11\bar{1})}{I_m(111) + I_m(11\bar{1}) + I_t(011)}$$

$$V_t = 1 - \frac{1.311X_m}{1 + 0.311X_m}$$

where the $I_m(111)$ and $I_m(11\bar{1})$ are the peak intensities of the (111) and $(11\bar{1})$ facets of the *m*-$ZrO_2$, and the $I_t(011)$ is the peak intensity of the (011) facet of the tetragonal $ZrO_2$. The average crystal sizes were estimated using the Jade 5.0 software at constant FWHM based on the XRD pattern profile fittings.

*Inductively-Coupled Plasma Atomic Emission Spectroscopy (ICP-AES).* The amounts of Na, Zr, and Pt of the $ZrO_2$ and Pt/$ZrO_2$ samples were determined using an ICP-AES system (ICP-AES, model Varian Inc.) at 589.592, 339.198, and 203.646 nm, respectively. The mixture of HF and aqua regia was used to dissolve the samples.


dx.doi.org/10.1021/cs300596q | ACS Catal. 2013, 3, 61−73

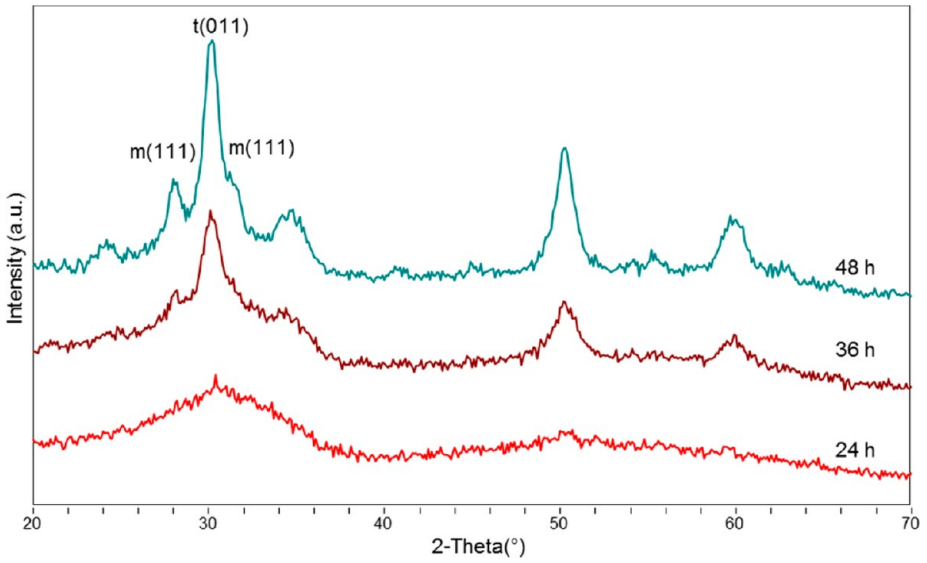


**Figure 1.** XRD patterns of the $ZrO_2$ samples after hydrothermal treatment at 120 °C for different time. Treatment condition: $ZrOCl_2{\cdot}8H_2O$ amount: 2 mmol, the molar ratio of $NH_4OH$: Zr = 4:1, total volume: 40 mL.

*X-ray Photoelectron Spectroscopy (XPS).* The binding energies and chemical shifts of the Na, Zr, and O species from the $ZrO_2$ samples were measured using a Thermo ESCALAB 250 Xi X-ray photoelectron spectrometer with an Al−K$\alpha$ radiation source. The $ZrO_2$ sample powders were loaded with a carbon tape disk on the top of a silicon wafer substrate and transferred into the vacuum prep chamber with overnight pumping before the measurement. The pass energies were 150 eV with 2 scans for the survey scan and 50 eV with 5 scans for the narrow scan. XPS Data was processed using the Thermo Avantage software.

*Thermogravimetric Analysis (TGA).* The as-synthesized t-$ZrO_2$ powders were analyzed using a TGA Q50 (TA Instruments) thermogravimetric analyzer for the organic decomposition study. Zero air was used as the purge gas. The sample purge flow was 90 mL/min, and the balance purge flow was 10 mL/min. Approximately 10 mg of sample was transferred into a platinum sample pan. The sample was heated from ambient to 900 °C at a ramp rate of 2 °C/min.

*High-Resolution Transmission Electron Microscopy (HRTEM).* The HRTEM images were obtained using a JEOL-2100F electron microscope operated at 200 kV. The TEM specimens were prepared using a two-step procedure. First, a tiny amount of sample was dispersed in ethanol and sonicated for 15 min. Then 3 drops of the suspension were deposited onto a 300 mesh Cu grid coated with a Lacey carbon film. The particle size distributions were obtained by measuring about 100−200 nanoparticles in several TEM images for each sample.

*Nitrogen Sorption.* The surface area measurement was carried out by $N_2$ physisorption. The $N_2$ adsorption and desorption isotherms were measured at a liquid $N_2$ temperature of 77 K using a Micromeritics 2720 system. The samples were outgassed at 473 K for 2 h prior to isotherm measurement. The specific surface areas were calculated using BET (Brunauer−Emmett−Teller) theory in the range of 0.05 to 0.3 of the relative pressure $P/P_0$.

**2.3. Hydrothermal Stability Test.** The hydrothermal stability of the Z600 t-$ZrO_2$ and the corresponding ALD Pt/Z600 sample was tested in different pH environments under autogenous autoclave reaction condition at 200 °C for 20 h. Liquid phase pH was adjusted using either HCl or NaOH to generate the final pH values. The total volume of the liquid mixture was kept constant at 70 mL. The autoclave was subsequently allowed to cool down to room temperature. The autoclave reaction mixture was then separated and washed exhaustively using absolute ethanol and DI water, and air-dried at 70 °C for 12 h. The white powders were collected for further characterization.

**2.4. Water-Gas-Shift Kinetic Measurements.** The WGS kinetic measurements were conducted in an automated, four-unit independent parallel tubular plug flow reactor setup as described elsewhere.[31] For each measurement, 200 to 400 mg of catalyst was loaded into the reactor. Prior to running the WGS reaction, the catalysts were reduced in 25% $H_2$/Ar with a flow rate of 50 sccm at 300 °C for 2 h, which was followed by a pretreatment at our standard WGS conditions (6.8% CO, 21.9% $H_2O$, 8.5% $CO_2$, 37.4% $H_2$, and balance Ar) with a flow rate of 75.4 sccm at 300 °C for 20 h to stabilize the catalysts. After the pretreatment stabilization, the temperature was lowered to the test temperature so that the conversion was less than 10% to guarantee the differential reaction conditions. A detailed discussion of the procedure for the WGS kinetic measurements was provided in our earlier work.[32,33] Briefly, the apparent reaction orders with respect to the reactants and products were measured by varying one gas concentration at a time (4−21% CO, 5−25% $CO_2$, 11−34% $H_2O$, and 14−55% $H_2$) at the test temperature, and the apparent activation energy was measured by varying the temperature over a range of 30 °C around the test temperature, with the concentrations kept constant at the standard conditions. The WGS reaction rate showed less than 10% decay of the initial rate during the kinetic measurements.

## 3. RESULTS AND DISCUSSION

**3.1. Effect of Synthesis Conditions on the Formation of $ZrO_2$.** *3.1.1. Phase Control: Effect of Hydrothermal Reaction Time.* We began with the study of the phase evolution of $ZrO_2$ using $NH_4OH$ as the mineralizer for hydrothermal synthesis at 120 °C at the fixed $NH_4OH$:Zr molar ratio of 4:1. Only a negligible amount of $ZrO_2$ was


dx.doi.org/10.1021/cs300596q | ACS Catal. 2013, 3, 61−73

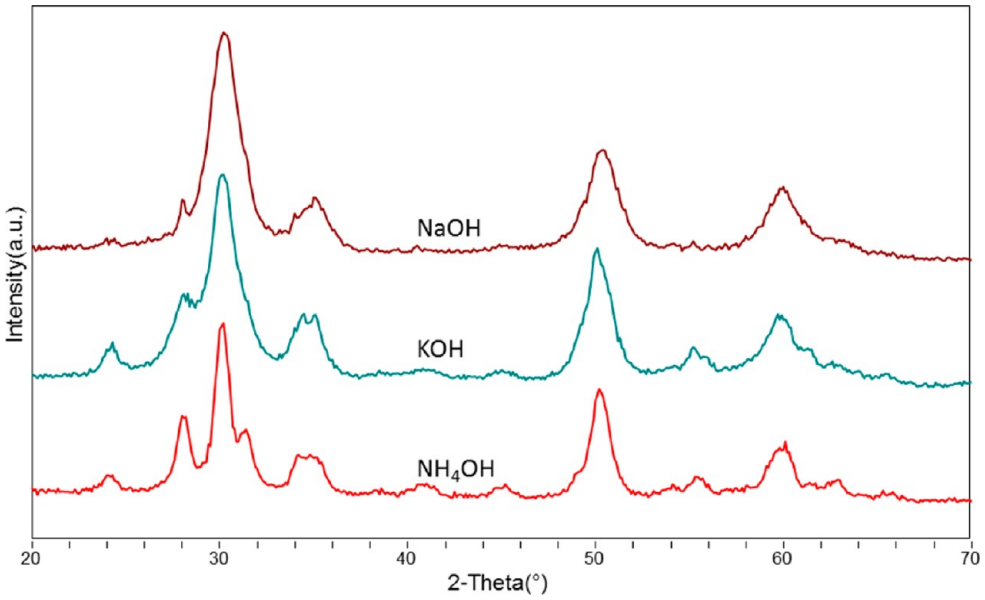


**Figure 2.** XRD patterns of $ZrO_2$ samples after hydrothermal synthesis reaction at 150 °C for 10 h using different mineralizers. The amount of $ZrOCl_2{\cdot}8H_2O$ was fixed at 2 mmol. The molar ratios were: $NH_4OH$:Zr = 70:1, KOH:Zr = 40:1 and NaOH:Zr = 100:1. Corresponding tetragonal phase amounts: 52% for $NH_4OH$, 66% for KOH and 90% for NaOH.

precipitated when the reaction time was less than 12 h. As shown in Figure 1, after 24 h treatment, amorphous $ZrO_2$ was formed, which was characterized by the two broad peaks centered at $2\theta$ = 30.4° and 50.8°. Extended treatments for 36 and 48 h resulted in the formation of tetragonal phase amounts of 84% and 61%, respectively. In a similar study (not shown), when NaOH was used as the mineralizer, keeping all the other synthesis conditions identical, the t-$ZrO_2$ amount decreased from 90% to 60% when increasing the treatment time from 10 to 20 h. Generally, the longer the treatment, the less the amount of the t-$ZrO_2$ formed. These results appear to suggest that the hydrous $ZrO_2$ precipitates were formed preferentially with tetragonal structure in the early stage of the synthesis process during the crystallization of amorphous hydrous zirconia as reported elsewhere.[17,22] Previous studies have shown that $ZrOCl_2{\cdot}8H_2O$ exists mainly in the form of cyclic $[Zr(OH)_2{\cdot}4H_2O]_4^{8+}$ tetramers in solution at room temperature. Upon heating or addition of base, these tetramers condense via olation and oxolation to form the corresponding polymers of $[ZrO_x(OH)_{4-2x}{\cdot}mH_2O]_n$ and ultimately hydrous $ZrO_2$ precipitates.[34] In this study, under hydrothermal synthesis conditions, in the presence of $OH^-$ from the base mineralizers, the hydrous $ZrO_2$ precipitates underwent the dissolution and precipitation process, which could induce the thermodynamically favorable reconstruction and transformation of metastable t-$ZrO_2$ to more stable m-$ZrO_2$ with extended reaction time. Therefore, it is crucial to control the synthesis time to obtain $ZrO_2$ with the desired phase.

*3.1.2. Phase Control: Mineralizer Effect.* From Figure.1, it is obvious that the reaction was slow at the temperature of 120 °C. We therefore conducted further synthesis at 150 °C to expedite the precipitation of crystalline $ZrO_2$. For this study, $NH_4OH$, KOH, and NaOH were tested as the mineralizers for the synthesis of the $ZrO_2$ nanoparticles. As shown in Figure 2, when $NH_4OH$ was the mineralizer, the product was about 50% monoclinic phase after hydrothermal reactions at 150 °C for 10 h, while using KOH, similar reaction conditions gave rise to a higher tetragonal amount of ~65%. The use of NaOH as the mineralizer significantly increased the tetragonal amount to 90% when the molar ratio of Zr precursor: NaOH was fixed at 1: 100. The nanoparticle sizes were ~5 nm in all cases as estimated by XRD. Table 1 summarizes the tetragonal phase amounts of the $ZrO_2$ formed using different amounts of mineralizers. These results clearly show that under similar reaction conditions, NaOH favored the formation of greater amounts of tetragonal $ZrO_2$ among these mineralizers, which is consistent with the observations from other groups.[21] A previous study has shown that increasing the mineralizer cation radius can cause a decrease in the crystallization rate of $ZrO_2$, which may allow sufficient time for the nucleation reaction to reach more thermodynamically stable m-$ZrO_2$.[35] The cation radius of $NH_4^+$, $K^+$, and $Na^+$ are: 0.148, 0.138, and 0.102 nm, respectively. Therefore, it is reasonable to obtain greater tetragonal amounts for $ZrO_2$ in our synthesis when NaOH was used as the mineralizer. On the basis of this finding, we continued further the preparation of tetragonal $ZrO_2$ using NaOH as the mineralizer.

**Table 1. Comparison of the Tetragonal Phase Percentage of the $ZrO_2$ Formed Using Different Mineralizers**

| mineralizer | ratio[a] | t-$ZrO_2$% |
|---|---|---|
| $NH_4OH$ | 10:1 | 41% |
| | 20:1 | 46% |
| | 70:1 | 52% |
| | 100:1 | 49% |
| KOH | 10:1 | 27% |
| | 20:1 | 66% |
| | 40:1 | 66% |
| | 80:1 | 38% |
| NaOH | 3:1 | 30% |
| | 40:1 | 65% |
| | 100:1 | 90% |

[a]The molar ratio of mineralizer:$ZrOCl_2{\cdot}8H_2O$


dx.doi.org/10.1021/cs300596q | ACS Catal. 2013, 3, 61−73

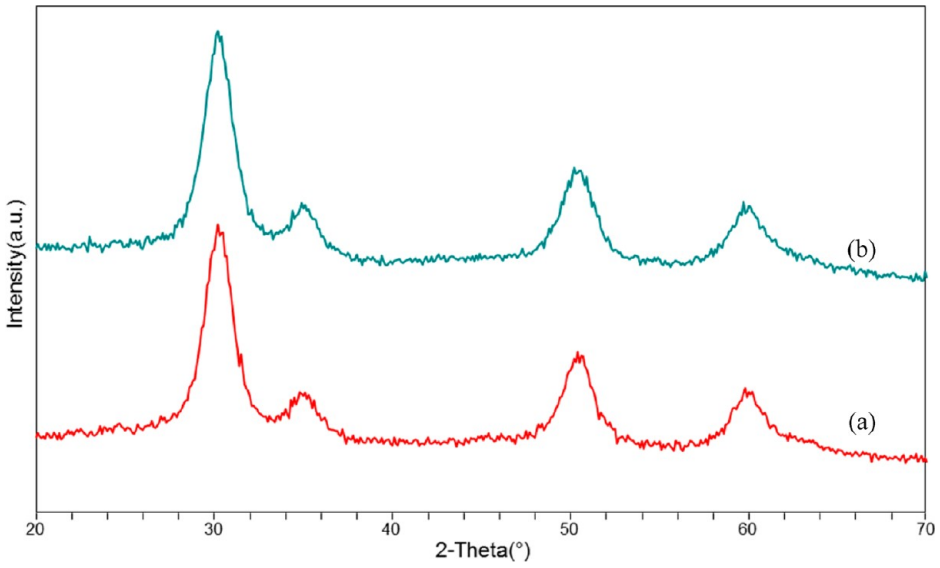


**Figure 3.** XRD patterns of the as-synthesized $ZrO_2$ nanoparticles: (a) with ethanol, (b) with oleic acid-ethanol. Synthesis condition: 5 mmol $ZrOCl_2 \cdot 8H_2O$ with 20 h hydrothermal treatment at 150 °C.

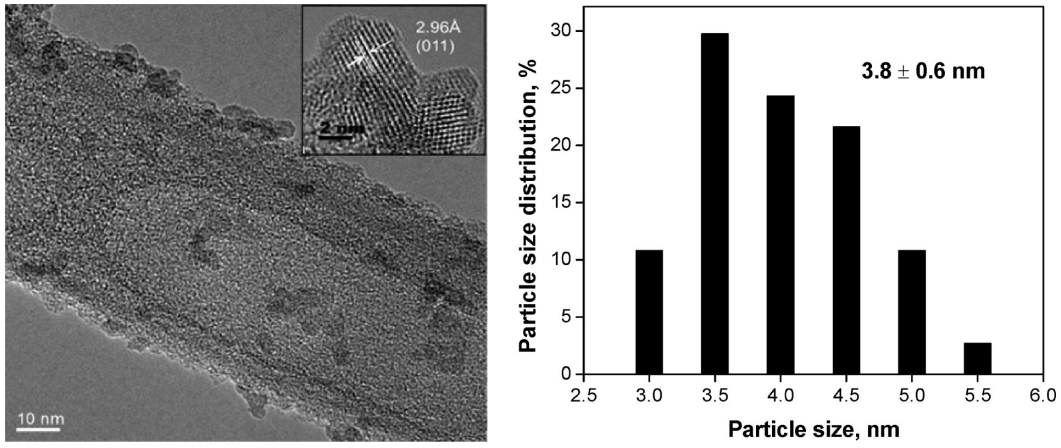


**Figure 4.** TEM measurement and particle size distribution of the as-synthesized t-$ZrO_2$ nanoparticles synthesized with oleic acid-ethanol. Synthesis condition: 5 mmol $ZrOCl_2 \cdot 8H_2O$ with 20 h hydrothermal treatment at 150 °C.

*3.1.3. Synthesis of t-$ZrO_2$ Nanocrystals.* To further increase the tetragonal percentage of the crystalline $ZrO_2$, we started to add organic additives into the reaction mixture for the hydrothermal treatment. The use of organic additives such as alcohol solvents along with surfactants including amines and carboxylic acids is common for metal oxide synthesis, for example, Rebuffetti et al. reported the use of ethanol and acetic acid for the synthesis of $SrTiO_3$.[36] Xu et al. reported the use of oleic acid, oleyamine, and *n*-octane for the synthesis of $ZrO_2$ while using zirconyl oleate as the Zr precursor.[37] Li et al. reported the use of methanol and $CO(NH_2)_2$ for the synthesis of $ZrO_2$ while using zirconyl nitrate as the Zr precursor.[22] Jiao et al. reported the preparation of $ZrO_2$ using polyhydric alcohol and di- and triethanolamine.[38] In accordance with these studies, we conducted the synthesis of t-$ZrO_2$ using the surfactant of oleic acid dissolved in ethanol. Furthermore, we used 5 mmol $ZrOCl_2 \cdot 8H_2O$ with 20 h hydrothermal treatment at 150 °C to increase the yield of the final t-$ZrO_2$. The molar ratios of reactants were Na:Zr = 40:1 and oleic acid:ethanol = 1:40. To further elucidate the function of oleic acid, similar syntheses without oleic acid were carried out as described in section 2.1.1.

As shown in Figure 3 by XRD analysis, the use of the oleic acid-ethanol/ethanol aqueous solution led to the formation of essentially pure tetragonal $ZrO_2$. The dielectric constants of water, oleic acid, and ethanol are 78.5, 2.5, and 24.5, respectively. Therefore, the dissolution of oleic acid-ethanol/ethanol in water can greatly decrease the dielectric constant of water. Similar to the effect of isopropyl alcohol on the synthesis of $ZrO_2$ using a homogeneous precipitation method as reported elsewhere;[17] in this study, the solubility of the Zr species in the oleic acid-ethanol/ethanol aqueous solution became lower when the dielectric constant of the solution was reduced by adding oleic acid-ethanol/ethanol to water. The presence of ethanol/oleic acid-ethanol therefore enhanced the particle formation kinetics, which could weaken the dissolution–precipitation process and prevent the subsequent phase transformation of the $ZrO_2$ precipitates from tetragonal to monoclinic phase. This weakening of the dissolution–precipitation process along with the use of NaOH mineralizer is likely to contribute to the formation of the tetragonal phase $ZrO_2$. However, the effect of oleic acid on the t-$ZrO_2$ formation was not obvious based on the XRD patterns. Although it was


dx.doi.org/10.1021/cs300596q | *ACS Catal.* 2013, 3, 61–73

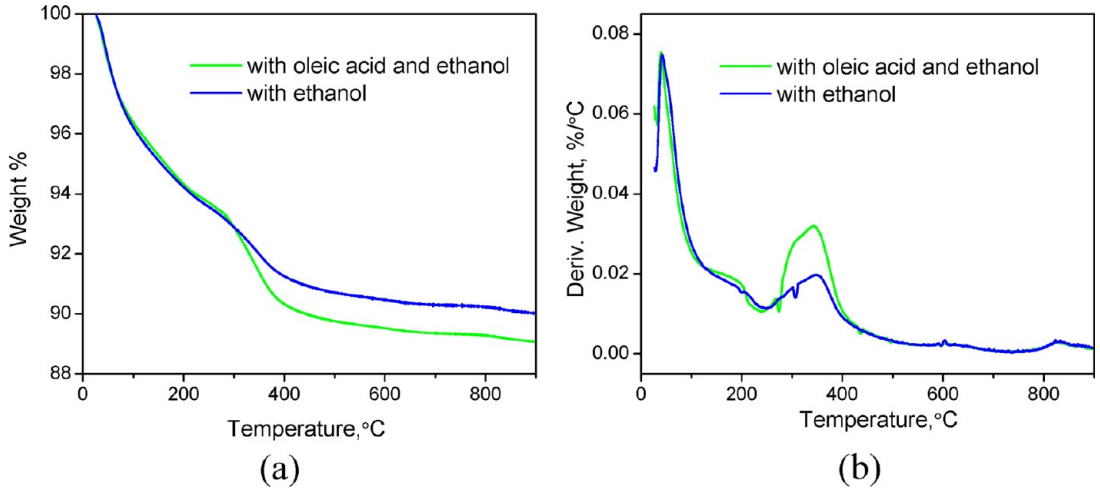


**Figure 5.** TGA measurement of the as-synthesized t-$ZrO_2$: (a) weight loss as a function of temperature, (b) derivative weight loss as a function of temperature.

reported by Xu et al.[37] that the use of a small amount of oleic acid may inhibit the attachment of nucleation seeds and therefore result in the formation of dispersed nanocrystals, such an inhibition effect is not clear based on our TEM measurement, as similar particle sizes and shapes were observed for these $ZrO_2$ samples. In both cases, the particle sizes of the as-synthesized t-$ZrO_2$ nanoparticles were ~3.8 nm based on TEM measurement (Figure.4). Furthermore, the HRTEM image showed a lattice spacing of 2.96 Å, which corresponds to the (011) facet of t-$ZrO_2$.

**3.2. Calcination of the As-Synthesized t-$ZrO_2$.** For catalysis application, it is necessary to remove the organic residues and impurities from the catalyst support materials that might have been introduced during the synthesis of the support. The decomposition of the organic residues including oleic acid and ethanol from the as-synthesized t-$ZrO_2$ was examined using TGA measurements. As shown in Figure 5, with the use of oleic acid surfactant during the hydrothermal treatment, the resulting as-synthesized $ZrO_2$ showed a significant weight loss of ~10% from 25 to 600 °C when being calcined in air (Figure 5a green line). Further temperature increase to 900 °C only resulted in an additional slight weight loss of 0.4%. In addition, the weight derivative showed sudden weight losses at ~40 and 350 °C, which correspond to the release of physisorbed $H_2O$ and $CO_2$ and the decomposition of the organic additives of oleic acid and ethanol, respectively (Figure 5b green line). With the use of ethanol solvent in the absence of oleic acid surfactant during the hydrothermal treatment, the resulting as-synthesized $ZrO_2$ showed similar results of weight and derivative weight losses to that in the presence of oleic acid surfactant (Figures 5a and 5b blue lines). On the basis of these similar XRD, TEM, and TGA results for the as-synthesized t-$ZrO_2$ samples, it is plausible that the use of oleic acid under our current studies did not change the nature of the t-$ZrO_2$ formation during the hydrothermal treatment in ethanol aqueous solution. The use of concentrated NaOH aqueous solution along with large amount of ethanol greatly outweighed the use of additional oleic acid for the formation of t-$ZrO_2$. The t-$ZrO_2$ samples formed through both approaches, that is, in the presence/absence of oleic acid, shared the same nature for the resulting t-$ZrO_2$. Differences between these t-$ZrO_2$ samples, if any, would be negligible. The following studies are based on the t-$ZrO_2$ synthesized using the oleic acid surfactant.

On the basis of the TGA results, the calcination of the as-synthesized t-$ZrO_2$ was further conducted at elevated temperatures of 300, 400, 500, 600, 700, and 800 °C in air separately for 3 h at each temperature. The calcined $ZrO_2$ samples are denoted accordingly as Z300, Z400, Z500, Z600, Z700, and Z800 $ZrO_2$, respectively. As shown in Figures 6a and 6b by XRD analyses, it is noticeable that the tetragonal phase of the $ZrO_2$ was stable up to 600 °C. Further increase of the calcination temperatures led to the appearance of monoclinic phase with decreasing amounts of tetragonal phase to 48% at 700 °C for Z700 and 15% at 800 °C for Z800, respectively, which was also accompanied by a simultaneous change of the nanocrystal sizes. As presented in Figure 6b, the $ZrO_2$ crystal sizes estimated from XRD pattern fittings show a gradual increase from 4.8 nm for Z300 to 6.8 nm for Z500. At higher calcination temperatures, the crystal sizes increased more sharply, as proved by an abrupt increase of the crystal sizes from ~11 nm for Z600 to ~25 nm and ~50 nm for Z700 and Z800, respectively.

The evolution of the crystal sizes for the t-$ZrO_2$ nanoparticles with calcination temperature was further characterized by TEM. As shown in Figure 7a, the crystal size and shape for the t-$ZrO_2$ after being calcined at 300 °C were essentially the same as those of the as-synthesized t-$ZrO_2$. The rough surface and agglomerated small particulates suggest that these irregularly shaped clusters were assemblies of small particulates ~4.2 nm. No obvious size change was observed after being calcined at 400 °C. However, these Z400 $ZrO_2$ nanoparticles started to form large agglomerates probably because of the removal of organic residues. More clear features of the nanoparticles were observed after being calcined at 500 °C with an average particle size of ~7.7 nm, which increased 56% to ~12 nm after being calcined at 600 °C (Figure 7b for Z600 $ZrO_2$). The nanoparticle sizes obtained by TEM measurement are consistent with the sizes estimated by XRD analyses, which were 4.8, 5.4, 6.8, and 11 nm for these Z300, Z400, Z500, and Z600 t-$ZrO_2$, respectively. Clearly, the decomposition of the organic residue dominated when the calcination was conducted at temperatures below 400 °C. In contrast, once the calcination temperature exceeded 400 °C, the $ZrO_2$ nanocrystals started to grow into larger particles that likely followed the Ostwald


dx.doi.org/10.1021/cs300596q | ACS Catal. 2013, 3, 61−73

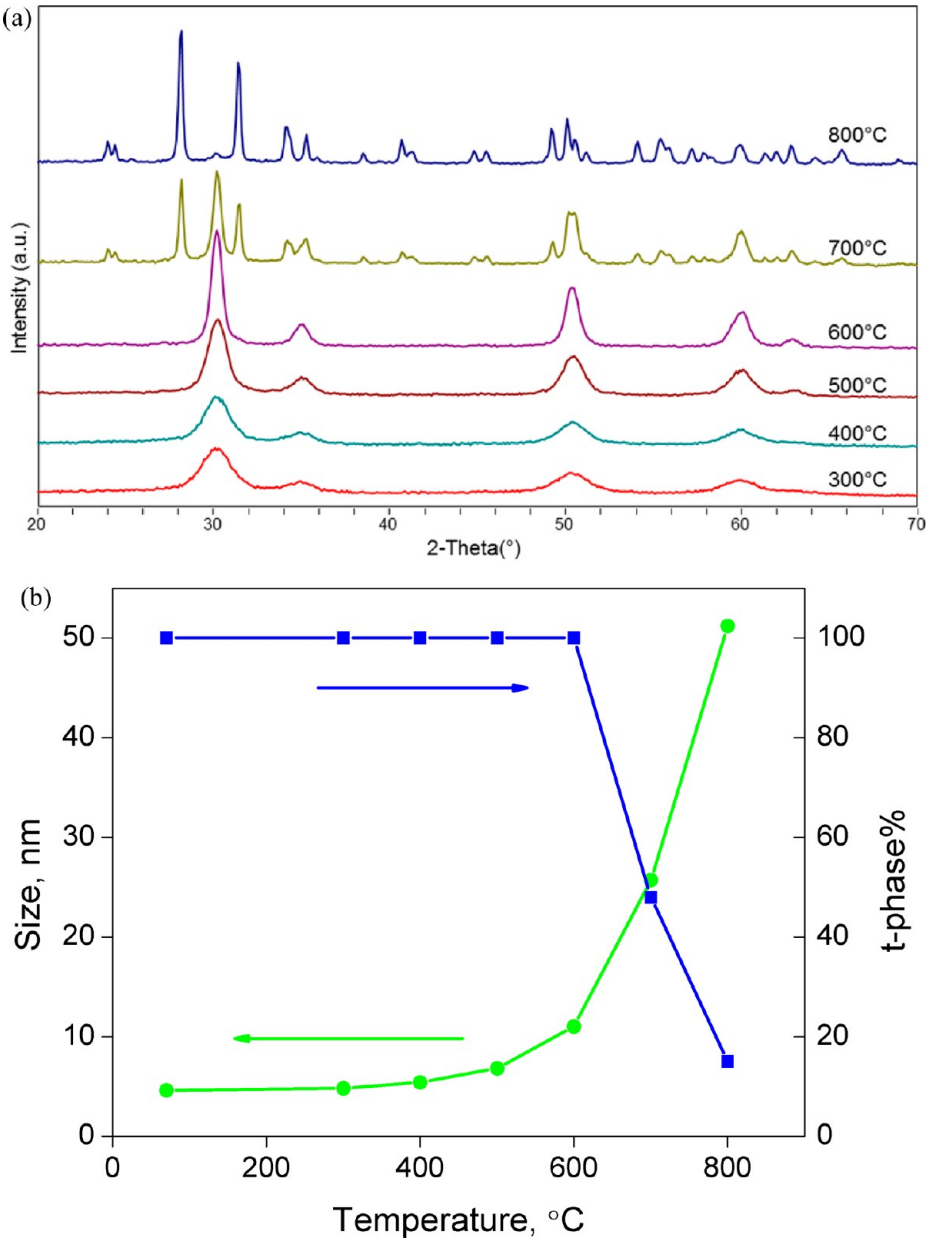


**Figure 6.** (a) XRD patterns of the Z300, Z400, Z500, Z600, Z700, and Z800 $ZrO_2$. (b) Tetragonal phase percentage and particle sizes of the Z300, Z400, Z500, Z600, Z700, and Z800 $ZrO_2$. Particle sizes were estimated by XRD pattern fittings.

ripening mechanism, by which small crystals or sol particles dissolve and redeposit onto the larger crystals to form larger particles. Indeed, the change of the particle sizes with temperatures followed a linear growth pattern in the temperature range of 400 to 600 °C. Higher temperatures expedited the crystal growth. Furthermore, HRTEM images show the clear lattice spacings of 0.295 and 0.297 nm (Figure 7c), corresponding to the (011) and (002) facets of t-$ZrO_2$. It is worth noting that, for the Z600 $ZrO_2$, it was still stabilized in the tetragonal phase without size and morphology changes after additional 3 h calcination at the same temperature. Further studies focus on the Z600 t-$ZrO_2$ based on these results.

**3.3. Pt/Z600 Catalyst by ALD.** One cycle ALD Pt was conducted using $MeCpPtMe_3$ as the Pt precursor at 300 °C on Z600 t-$ZrO_2$. The Pt/Z600 sample thus prepared was further oxidized in 10% $O_2$/Ar at 300 °C for 30 min and reduced in 10% $H_2$/Ar at 280 °C for 30 min to reach the final catalyst. As shown in Figure 8, monodispersed Pt nanoparticles ~2.5 nm were obtained for the unreduced Pt/Z600 sample. The reduction of the Pt/Z600 led to a decrease in the Pt nanoparticle size to ~1.5 nm, which suggests that the oxidation−reduction treatment of the unreduced Pt/Z600 may cause a redistribution of the Pt species on the Z600 t-$ZrO_2$ to form smaller Pt nanoparticles.

**3.4. Hydrothermal Stability of the Z600 t-$ZrO_2$ and ALD Pt/Z600.** To further investigate the feasibility of the Z600 t-$ZrO_2$ as a catalyst support for liquid phase reaction application, the hydrothermal stability of the Z600 t-$ZrO_2$ was tested at 200 °C under aqueous autoclave reaction conditions for 20 h at different pH environments of pH = 1, 4.5, 5, and 13. The pH values of 1, 5, and 13 were adjusted by adding HCl, $H_2O$, and NaOH into the aqueous suspension of Z600, respectively, while the pH of 4.5 was adjusted by adding glycerol into the Z600 and water suspension. The hydrothermal


dx.doi.org/10.1021/cs300596q | ACS Catal. 2013, 3, 61−73

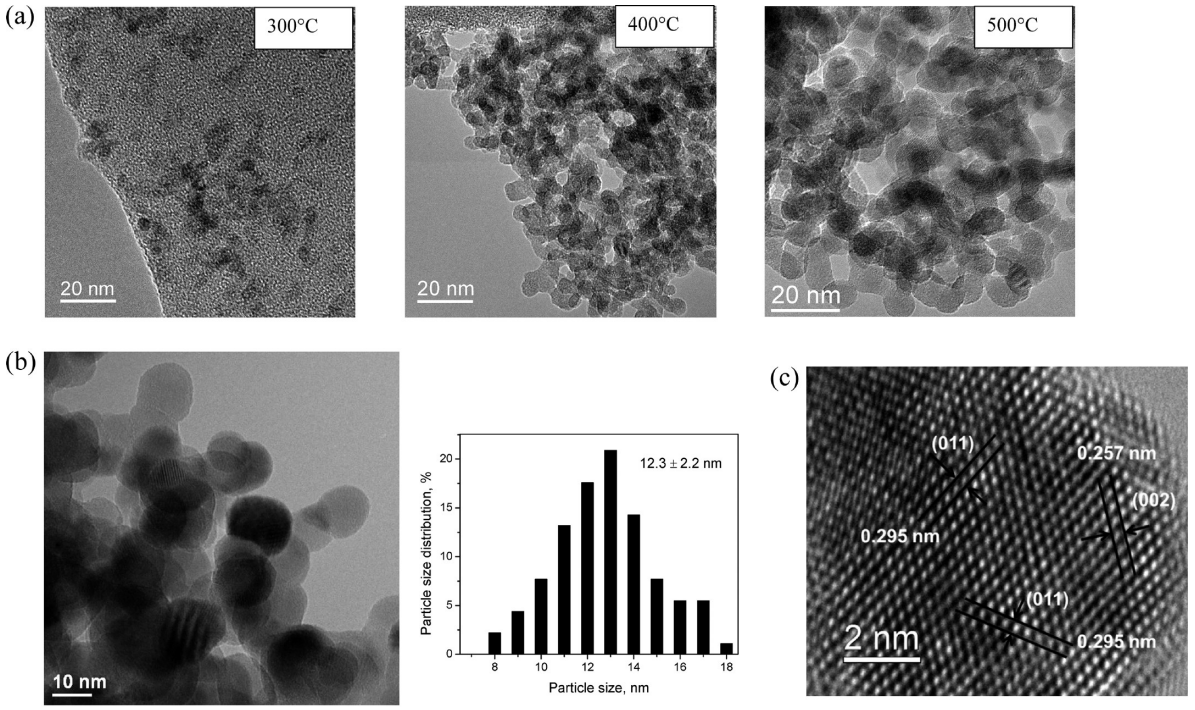


**Figure 7.** (a) TEM images for the Z300, Z400, and Z500 t-$ZrO_2$. (b) TEM image and particle size distribution for the Z600 t-$ZrO_2$. (c) HRTEM image for the Z600 t-$ZrO_2$.

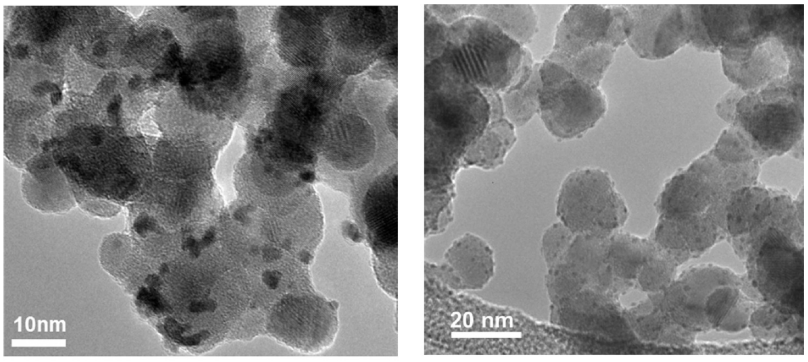


(a) (b)

**Figure 8.** TEM images for Pt/Z600 prepared by ALD method (a) before reduction, (b) after reduction.

stability of the unreduced Pt/Z600 sample was also tested at 200 °C under aqueous autoclave reaction conditions for 20 h at the pH of 4.5, which was adjusted by HCl.

As shown in Figure 9, regardless of the different pH environments of the test conditions, all the samples after these tests showed a similar XRD pattern of the Z600 t-$ZrO_2$ with an XRD estimated particle size of ~12 nm. No pronounced Pt peaks were observed for the Pt/Z600 sample, which confirms that the Pt nanoparticles formed by ALD were small (<5 nm) and did not increase notably in size as a result of the hydrothermal treatments.

Moreover, all these Z600 t-$ZrO_2$ samples after hydrothermal tests showed similar $N_2$ adsorption−desorption isotherms (Figure 10). According to the IUPAC classification, these isotherms correspond to the Type IV isotherm with a H3 hysteresis loop that can be found in solids consisting of plate-like particles. The BET surface areas ($S_{BET}$) for these samples are listed in Table 2. In particular, the $S_{BET}$ for Z600 was 55 $m^2/g$. The change of the pH environments of the test conditions had no obvious influence on the surface areas which remained essentially constant at ~59 $m^2/g$. Further ICP-AES analyses of the unreduced Pt/Z600 sample showed the same Pt loading of ~3.9 wt % before and after the hydrothermal stability test at pH= 4.5. In addition, negligible, if any, Pt sintering or leaching was observed from the TEM images for the unreduced Pt/Z600 sample after the hydrothermal test (Figure 11) compared to the Pt/Z600 sample before the test (Figure 8a). The TEM average particle size was ~2.5 nm (Figure 11), which is similar to that of the Pt/Z600 sample before hydrothermal treatment (Figure 8a). These results clearly suggest that the Z600 t-$ZrO_2$ and the Pt/Z600 sample had superior hydrothermal stability, which may have great potential for liquid phase reaction application.

**3.5. Na Stabilization of the Tetragonal Phase $ZrO_2$.** The results so far indicate that the combined use of controlled hydrothermal synthesis and calcination process led to the formation of pure tetragonal phase $ZrO_2$ with crystal size ~12 nm that showed exceptional air and hydrothermal stability. It is


dx.doi.org/10.1021/cs300596q | ACS Catal. 2013, 3, 61−73

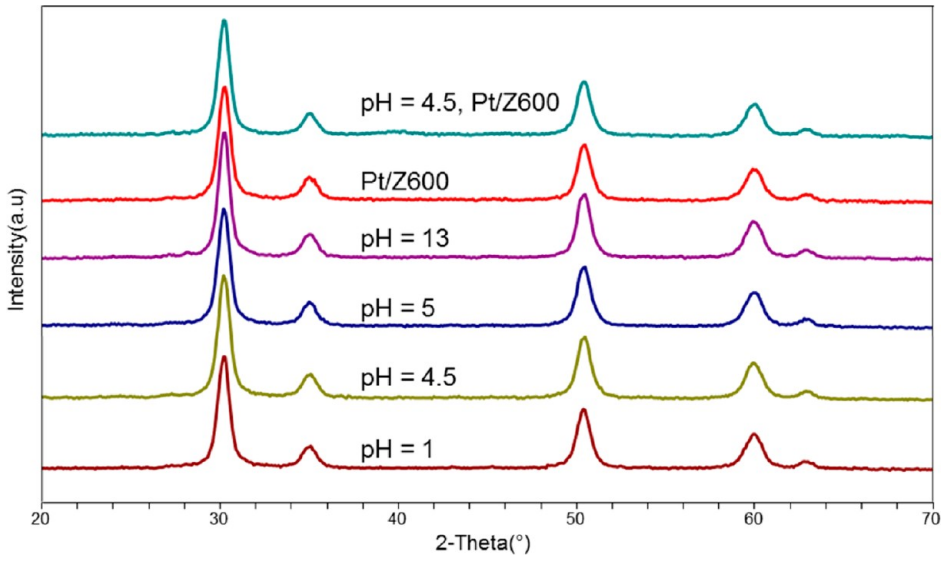


**Figure 9.** XRD patterns of the Z600 and Pt/Z600 after autoclave hydrothermal stability tests in different pH environments at 200 °C for 20 h.

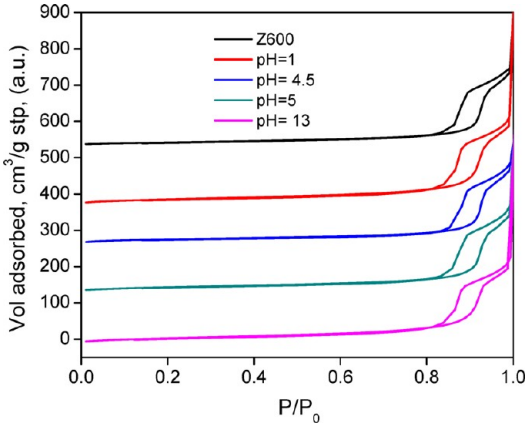


**Figure 10.** $N_2$ adsorption/desorption isotherms measured at 77 K for the Z600 $ZrO_2$ after autoclave hydrothermal stability tests in different pH environments at 200 °C for 20 h.

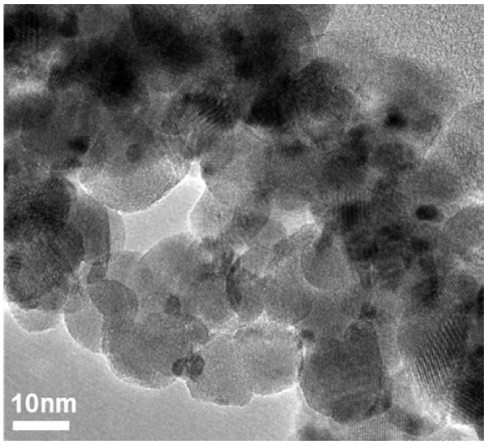


**Figure 11.** TEM images for the unreduced Pt/Z600 sample after autoclave hydrothermal stability test at pH = 4.5 and 200 °C for 20 h.

**Table 2. Specific Surfaces Area of the Z600 $ZrO_2$ before and after Autoclave Hydrothermal Stability Tests in Different pH Environments**

| pH | Z600 | 1 | 4.5 | 5 | 13 |
|---|---|---|---|---|---|
| $S_{BET}$, $m^2/g$ | 55 | 64 | 52 | 58 | 62 |

well-known that t-$ZrO_2$ is metastable at low temperature and will tend to transform to m-$ZrO_2$. Models of t-$ZrO_2$ stabilization at room temperature were reviewed by Stefanic et al.[39] The anionic impurities, particle size, lattice defects, and water vapor all have been reported to influence the tetragonal phase stability of $ZrO_2$. It has been a matter of controversy for the stabilization mechanism of the metastable tetragonal phase of $ZrO_2$. For instance, Xie et al. reported that 80% of t-$ZrO_2$ was transformed to m-$ZrO_2$ upon contact with water at room temperature,[14] while Wang et al. reported that t-$ZrO_2$ nanostructure partially transformed into m-$ZrO_2$ with the removal of the hydrated surface layers. For the synthesis of undoped $ZrO_2$, based on XRD estimation, Garvie proposed that there appeared to be a critical crystallite size of ~30 nm, above which the metastable tetragonal phase $ZrO_2$ could not exist at room temperature.[20] In contrast, Shukla et al. reported the $ZrO_2$ nanocrystallites with a size of ~45 nm were responsible for the metastable tetragonal phase stabilization at room temperature within the submicrometer sizes.[15] In most practical applications, doped divalent or trivalent cations such as $Ca^{2+}$ and $Y^{3+}$ are commonly introduced to stabilize the metastable tetragonal phase of t-$ZrO_2$.[23,24] The stabilization is interpreted as due to the decrease in the coordination number of the $Zr^{4+}$ ion caused by the incorporation of aliovalent dopant cations.[40] In our studies, no specific stabilizer was introduced during the hydrothermal synthesis. It is therefore very intriguing to understand the mechanism that led to the formation of the stable t-$ZrO_2$ in the absence of typical transition metal oxide stabilizers.

For the preparation of porous $ZrO_2$, Chuah et al. proposed that Na ions were preferentially absorbed into the $ZrO_2$ lattice during strong base digestion to stabilize $ZrO_2$ in the tetragonal phase based on atomic absorption spectroscopy analysis. However, their Na containing $ZrO_2$ treated at 1000 °C was not fully dissolved by the concentrated sulfuric acid, which may have led to the incomplete recovery of the Na amount by atomic adsorption analysis.[18] Prastomo et al. also proposed a Na ion stabilization mechanism for porous $ZrO_2$ preparation based on energy dispersive X-ray spectroscopy analysis.[16] In


dx.doi.org/10.1021/cs300596q | ACS Catal. 2013, 3, 61−73

another study, Song et al. used $NH_3$ solution to form a hydrogel before the subsequent hydrothermal synthesis using NaOH mineralizer.[27] They discussed the NaOH concentration effect on the phase transformation of $ZrO_2$ after hydrothermal treatment and found that low concentrations of NaOH (<2 wt %) favored the formation of t-$ZrO_2$ while increasing the NaOH concentration (5−40 wt %) favored the formation of m-$ZrO_2$. In this study, we investigated the Na effect on the $ZrO_2$ phase formation for the calcined $ZrO_2$ prepared through hydrothermal synthesis. For this purpose, the initial concentrations of NaOH were fixed at 2.5 and 10 M, keeping all the other hydrothermal reaction conditions intact and following the same calcination process from 400 to 800 °C. As shown in Figure 12a, the 10 M NaOH led to an overall greater tetragonal

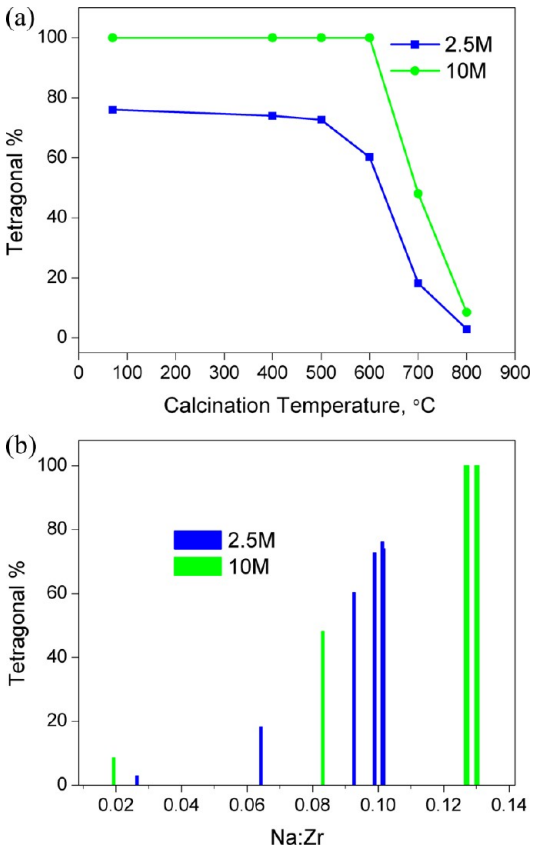


**Figure 12.** (a) Tetragonal phase percentage as a function of initial NaOH concentration at different calcination temperatures. (b) The tetragonal phase percentage as a function of Na amount. The molar ratio of Na:Zr was defined as the molar ratio between Na and Zr and was measured by ICP-AES.

percentage compared to the 2.5 M NaOH regardless of the calcination temperatures. Indeed, the use of the 2.5 M NaOH failed to produce pure tetragonal $ZrO_2$, and the tetragonal amounts decreased with calcination temperatures while using the 2.5 M NaOH. These results validate the use of the relatively higher initial concentration of the 10 M NaOH for the preparation of the pure tetragonal phase $ZrO_2$. The amounts of the Na and Zr species for these $ZrO_2$ samples were further measured by ICP-AES. As shown in Figure 12b, the tetragonal percentages increased with the Na amounts. Pure tetragonal phase $ZrO_2$ could be obtained at the molar ratio of Na:Zr = ~0.13:1. Below this ratio, only a mixture of monoclinic and tetragonal phases of $ZrO_2$ was obtained.

The surface amounts of the Zr, Na, and O species for Z600, Z700, and Z800 $ZrO_2$ were analyzed by XPS. Similar binding energies were observed for these samples by the XPS survey scans and narrow scans (Figures 13 and 14). As shown in

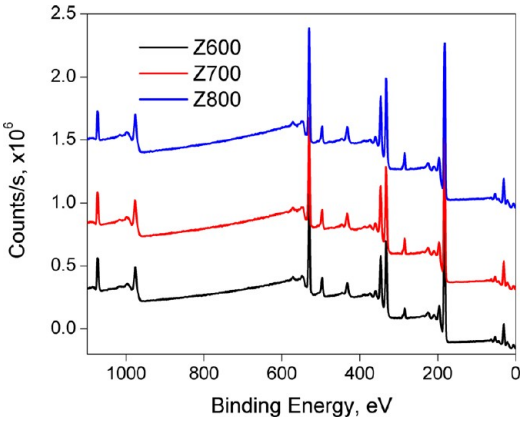


**Figure 13.** XPS survey scans for the calcined $ZrO_2$ on silicon wafer substrate at room temperature.

Figure 13, no Cl signal was detected from these $ZrO_2$ samples, which confirms the effectiveness of Cl removal during the exhaustive washing procedure. The binding energy values were ~181.9 eV, ~1073.1 eV, and ~530.5 eV for Zr, Na, and O species (Figure 14), respectively, which suggest that the Zr, Na, and O species were in the form of $ZrO_2$ and $Na^+$ ions.[41,42] The amounts of surface Na, Zr, and O were quantified with XPS narrow scans (Table 3a). The results (in molar percentage) reveal only negligible changes in the surface Zr amounts. However, ~8% and ~20% Na losses were detected from Z600 to Z700 and Z800, respectively. In addition, the amounts of bulk Na, Zr, and O were quantified with ICP-AES (Table 3b). The results also show only negligible changes of the bulk Zr amounts from the surface Zr amounts. However, ~36% and ~84% bulk Na losses were detected from Z600 to Z700 and Z800, respectively. Moreover, the Z700 and Z800 showed about 4-fold greater Na losses from the bulk than that from the surface, that is, 36% vs 8% for Z700 and 84% vs 20% for Z800, respectively. The ratios of surface $(Na:Zr)_{XPS}$:bulk $(Na:Zr)_{ICP\text{-}AES}$ for Z600, Z700, and Z800 calculated based on the data from Table 3 were 2.6, 3.7, and 13, respectively. These results show that, in general, the surface had greater amounts of Na than the bulk, regardless of the tetragonal contents of these $ZrO_2$. Compared to the bulk, the surface showed less severe Na loss, while the Na loss was significant from the bulk. It is therefore plausible that the surface Na was more stable than the bulk Na, and it was the Na incorporated into the internal $ZrO_2$ structure that helped maintain the stability of the tetragonal phase of the Z600 $ZrO_2$.

**3.6. Water-Gas-Shift Reaction Kinetics.** The Z600 t-$ZrO_2$ and m-$ZrO_2$ were used as the supports for catalyst preparation. The catalysts for WGS reaction kinetic measurements include 2.0% Pt/t-$ZrO_2$, 3.9% Pt/t-$ZrO_2$, 0.6% Pt/m-$ZrO_2$, and 5.9% Pt/m-$ZrO_2$. The WGS reaction rates are listed in Table 4. The reaction rates were calculated based on the mass of catalyst, the total moles of Pt, and the exposed moles of Pt for these catalysts at 250 °C and our standard WGS conditions (1 atm total pressure, 6.8% CO, 21.9% $H_2O$, 8.5% $CO_2$, 37% $H_2$ and balance Ar). The apparent activation energies and reaction orders for these catalysts are listed in Table 5. The


dx.doi.org/10.1021/cs300596q | ACS Catal. 2013, 3, 61−73

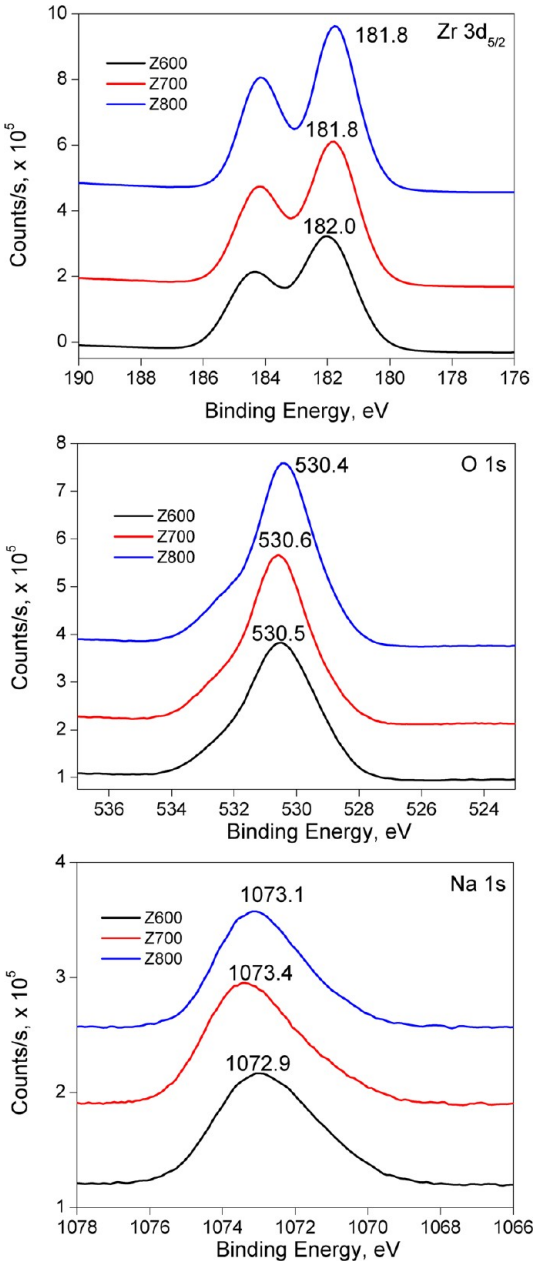


**Figure 14.** XPS narrow scans for the Zr, O, and Na species from the calcined $ZrO_2$ on silicon wafer substrate at room temperature.

**Table 3. XPS (a) and ICP-AES (b) Element Analysis for the Calcined $ZrO_2$**

| sample | tetragonal | Na | Zr | O | Na:Zr |
|---|---|---|---|---|---|
| | | (a) XPS Element Analysis | | | |
| Z600 | 100% | 10.7% | 31.2% | 58.1% | 0.34 |
| Z700 | 48.1% | 9.8% | 31.8% | 58.4% | 0.31 |
| Z800 | 8.5% | 8.4% | 32.4% | 59.2% | 0.26 |
| | | (b) ICP-AES Element Analysis | | | |
| Z600 | 100% | 4.2% | 31.9% | 63.9%[a] | 0.13 |
| Z700 | 48.1% | 2.7% | 32.4% | 64.9%[a] | 0.08 |
| Z800 | 8.5% | 0.65% | 33.1% | 66.2%[a] | 0.02 |

[a]Amount was approximated with 2-fold of Zr amount based on Zr:O = 1:2 for $ZrO_2$.

apparent activation energies were determined by measuring the WGS rates over these catalysts within a temperature range of ±15 °C around the test temperature at our standard WGS feed composition. The reaction orders were determined by measuring the WGS rates over these catalysts within a range of partial pressures of a reactant or a product while keeping the other partial pressures constant at the test temperatures. This procedure has been described in detail in the Experimental Methods section. It is noted that the apparent reaction orders reported in Table 5 were determined at different temperatures because the rates per gram of these catalyst varied by a factor of 18. Therefore, to achieve differential conditions (CO conversions less than 10%) it was necessary to test the catalysts with a higher rate per gram at lower temperatures. It should also be noted that the m-$ZrO_2$ supported catalysts did not contain Na, whereas, the t-$ZrO_2$ supported catalysts had Na contents as analyzed previously.

The 0.6% Pt/m-$ZrO_2$ and 5.9% Pt/m-$ZrO_2$ catalysts had 100% and 40% of the Pt exposed, which correspond to Pt nanoparticle sizes of 1.1 and 2.7 nm, respectively. Table 4 shows that the WGS turnover rate (TOR) for these two m-$ZrO_2$ supported Pt/$ZrO_2$ catalysts at 250 °C were both ∼7.0 × $10^{-2}$ $s^{-1}$, independent of the Pt particle size and loading. Similar results were obtained in the cases of Pt/$Al_2O_3$, Pt/$TiO_2$, and Pt/$CeO_2$ catalysts, where the WGS TOR was found to be independent of Pt weight loading and Pt particle size.[44] Indeed, for the two t-$ZrO_2$ supported 2.0% Pt/t-$ZrO_2$ and 3.9% Pt/t-$ZrO_2$ catalysts, the TORs at 250 °C were essentially the same ∼37 × $10^{-2}$ $s^{-1}$, regardless of different preparation methods, which were ∼5 times higher than the TORs for Pt/m-$ZrO_2$ catalysts without Na (Table 4). To investigate the Na effect on Pt/$ZrO_2$ catalyst for WGS reaction, we prepared Pt/Na/m-$ZrO_2$ catalysts following the same sequential impregnation and co-impregnation of Pt and Na protocols as described elsewhere.[45−47] However, contrary to the report that the WGS reaction rates for Pt/$Al_2O_3$, Pt/$SiO_2$, and Pt/$TiO_2$ catalysts were promoted by the addition of Na,[45−47] no WGS TOR was increased in these Pt/Na/m-$ZrO_2$ catalysts.

In addition to the changes in TORs, we also observed the changes in the reaction orders (Table 5) for $H_2O$ (∼0.7 to 0.81), $H_2$ (∼-0.5 to ∼-0.24), CO (0.12 to −0.15), $CO_2$ (∼0 to ∼-0.13) and an increase in $E_a$ by ∼20 kJ·$mol^{-1}$ for Pt/t-$ZrO_2$ catalysts compared to the Pt/m-$ZrO_2$ catalysts without Na. Similar change trends were reported by Pazmiño et al. for Pt/Na/$Al_2O_3$ and Pt/Na/$TiO_2$ catalysts under WGS reaction conditions, where increases in $H_2O$ and $H_2$ orders and decreases in CO and $CO_2$ orders along with higher $E_a$ were observed compared to their counterparts without Na.[45] The similar trends in the changes of the reaction orders and apparent activation energies between our Pt/t-$ZrO_2$ and the reported Pt/Na/$Al_2O_3$ and Pt/Na/$TiO_2$ catalysts suggest that the promotion in TORs by the Pt/t-$ZrO_2$ catalysts, compared to Pt/m-$ZrO_2$ catalysts without Na, could be due to the presence of Na. The fact that no promotion was observed in the Pt/Na/m-$ZrO_2$ catalysts compared to the Pt/m-$ZrO_2$ catalyst, suggests, albeit further studies are needed, that the increase in the WGS reaction rate with the Pt/t-$ZrO_2$ catalysts may be related to the phase difference between the two $ZrO_2$ supports, that is, tetragonal phase t-$ZrO_2$ versus monoclinic m-$ZrO_2$.

More significantly, the absolute values of reaction orders ($H_2O$ ∼0.8, $H_2$ ∼-0.2, CO ∼-0.1, and $CO_2$ ∼-0.13) and apparent activation energies (∼90 kJ·$mol^{-1}$) for the Pt/t-$ZrO_2$


dx.doi.org/10.1021/cs300596q | ACS Catal. 2013, 3, 61−73

Table 4. WGS Reaction Rate of $Pt/ZrO_2$ Catalysts[a]

| catalyst | rate per gram of catalyst ($\times 10^{-6}$ mol $g^{-1}$ $s^{-1}$) | rate per total mole of Pt ($\times 10^{-2}$ $s^{-1}$) | percentage of metal exposed[d] (D%) | estimated Pt particle size[e] ($d$, nm) | TOR ($\times 10^{-2}$ $s^{-1}$) |
|---|---|---|---|---|---|
| 2.0% Pt/t-$ZrO_2$[b] | 13 | 13 | 38 | 2.8 | 34 |
| 3.9% Pt/t-$ZrO_2$[c] | 40 | 22 | 55 | 2.0 | 40 |
| 0.6% Pt/m-$ZrO_2$[c] | 2.2 | 7.1 | 100 | 1.1 | 7.1 |
| 5.9% Pt/m-$ZrO_2$[c] | 7.8 | 2.7 | 40 | 2.7 | 6.8 |

[a]at 250°C, 1 atm Total Pressure, 6.8% CO, 21.9% $H_2O$, 8.5% $CO_2$, 37% $H_2$, and Balance Ar. [b]Prepared by IWI. [c]Prepared by ALD. [d]Determined by $H_2/O_2$ titration. [e]Particle size was estimated by $d = 108/(D\%)$.[43]

Table 5. WGS Reaction Kinetics on Supported Pt Catalysts

| | | | reaction order (±0.03) | | | |
|---|---|---|---|---|---|---|
| catalyst | $E_a$ (kJ·$mol^{-1}$) | temperature[c] (°C) | CO | $H_2O$ | $CO_2$ | $H_2$ |
| 2.0% Pt/t-$ZrO_2$[a] | 93 | 185 | −0.15 | 0.81 | −0.09 | −0.21 |
| 3.9% Pt/t-$ZrO_2$[b] | 93 | 180 | −0.15 | 0.81 | −0.18 | −0.27 |
| 0.6% Pt/m-$ZrO_2$[b] | 72 | 230 | 0.12 | 0.63 | 0.00 | −0.45 |
| 5.9% Pt/m-$ZrO_2$[b] | 72 | 210 | 0.12 | 0.75 | 0.00 | −0.51 |

[a]Prepared by IWI. [b]Prepared by ALD. [c]Temperature at which the reaction order measurements were carried out.

were similar to that of the reported $Pt/Na/Al_2O_3$ and $Pt/Na/TiO_2$ catalysts.[45] This suggests that the nature of active sites for these catalysts was similar: the Pt remained in the metallic state and served as a conduit to adsorb CO for it to react with other intermediates generated on the support.[45] On the basis of these similar kinetic results, the Na in t-$ZrO_2$ was likely to modify the support (not Pt) properties to create new active sites that promoted the WGS reaction as postulated in the case of $Pt/Na/Al_2O_3$ and $Pt/Na/TiO_2$ catalysts.[45]

While the nature of the active sites and the cause of promotion of TOR by Na have been discussed, the data in this work are not sufficient to determine the WGS reaction mechanism over these catalysts. The discussion of reaction mechanism is beyond the scope of our current work and will be the focus of our future work.

In summary, owing to the presence of Na in Pt/t-$ZrO_2$ as compared to the Pt/m-$ZrO_2$ catalysts, the WGS TORs were promoted by a factor of ∼5. The apparent reaction orders and activation energies of the Pt/t-$ZrO_2$ catalysts are similar to those of $Pt/Na/Al_2O_3$ and $Pt/Na/TiO_2$ catalysts reported in the literature. On the basis of the WGS kinetics over these catalysts, metallic Pt particles were the active sites for the WGS reaction on Na-containing Pt/t-$ZrO_2$ catalysts, and the WGS reaction promotion effect was due to the modification of the support by Na.

## 4. CONCLUSIONS

Nonporous t-$ZrO_2$ catalyst support with well-defined shape, size, and superior hydrothermal stability was prepared by a controlled hydrothermal synthesis approach with an optimized calcination process. The formation of the tetragonal phase of $ZrO_2$ during hydrothermal treatment was primarily due to the utilization of concentrated NaOH solution along with ethanol solvent. The use of oleic acid surfactant resulted in the formation of t-$ZrO_2$ of essentially identical nature. Pt nanoparticles ∼1.5 ± 0.3 nm were obtained using the Z600 t-$ZrO_2$ as the catalyst support for the preparation of Pt/t-$ZrO_2$ catalyst via the Pt ALD method. In addition, Na ions were found to incorporate into the t-$ZrO_2$ structure to stabilize the $ZrO_2$ in the tetragonal phase. While Na did not promote the Pt/m-$ZrO_2$ catalyst for the WGS reaction, the WGS TORs were promoted by a factor of ∼5 because of the presence of Na in Pt/t-$ZrO_2$ catalysts as compared to the Pt/m-$ZrO_2$. The metallic Pt were the active sites for the WGS reaction on Na-containing Pt/t-$ZrO_2$ catalysts. These results suggest that t-$ZrO_2$ is a promising catalyst support material for liquid phase biomass reforming applications.

## AUTHOR INFORMATION


### Corresponding Author

*E-mail: krp@northwestern.edu.

### Present Address

[‖]The Dow Chemical Company, Freeport, TX, U.S.A.


### Notes

The authors declare no competing financial interest.

## ACKNOWLEDGMENTS

This material is based upon work supported as part of the Institute for Atom-efficient Chemical Transformations (IACT), an Energy Frontier Research Center funded by the U.S. Department of Energy, Office of Science, Office of Basic Energy Sciences. We thank Mr. Yuyuan Lin for helping with HRTEM images.

## REFERENCES


(1) Yamaguchi, T. *Catal. Today* **1994**, *20*, 199−218.
(2) Yamaguchi, T.; Sasaki, H.; Tanabe, K. *Chem. Lett.* **1973**, 1017−1018.
(3) Davis, B. H. *Appl. Surf. Sci.* **1984**, *19*, 200−218.
(4) Abe, H.; Maruya, K.; Domen, K.; Onishi, T. *Chem. Lett.* **1984**, 1875−1878.
(5) He, M. Y.; Ekerdt, J. G. *J. Catal.* **1984**, *87*, 381−388.
(6) Ma, Z.-Y.; Yang, C.; Wei, W.; Li, W.-H.; Sun, Y.-H. *J. Mol. Catal A: Chem.* **2005**, *231*, 75−81.
(7) Nakano, Y.; Yamaguchi, T.; Tanabe, K. *J. Catal.* **1983**, *80*, 307−314.
(8) Lei, T.; Xu, J. S.; Tang, Y.; Hua, W. M.; Gao, Z. *Appl. Catal., A* **2000**, *192*, 181−188.
(9) Stichert, W.; Schüth, F.; Kuba, S.; Knözinger, H. *J. Catal.* **2001**, *198*, 277−285.
(10) Roh, H.-S.; Jun, K.-W.; Dong, W.-S.; Chang, J.-S.; Park, S.-E.; Joe, Y.-I. *J. Mol. Catal A: Chem.* **2002**, *181*, 137−142.
(11) Jin, G.; Lu, G.; Guo, Y.; Guo, Y.; Wang, J.; Liu, X. *Catal. Today* **2004**, *93*−*95*, 173−182.
(12) Shukla, S.; Seal, S. *J. Phys. Chem. B* **2004**, *108*, 3395−3399.

(13) Chary, K. V. R.; Ramesh, K.; Naresh, D.; Rao, P. V. R.; Rao, A. R.; Rao, V. V. *Catal. Today* **2009**, *141*, 187−194.
(14) Xie, S.; Iglesia, E.; Bell, A. T. *Chem. Mater.* **2000**, *12*, 2442−2447.
(15) Shukla, S.; Seal, S.; Vij, R.; Bandyopadhyay, S.; Rahman, Z. *Nano Lett.* **2002**, *2*, 989−993.
(16) Prastomo, N.; Muto, H.; Sakai, M.; Matsuda, A. *Mater. Sci. Eng., B* **2010**, *173*, 99−104.
(17) Hu, M. Z. C.; Hunt, R. D.; Payzant, E. A.; Hubbard, C. R. *J. Am. Ceram. Soc.* **1999**, *82*, 2313−2320.
(18) Chuah, G. K.; Jaenicke, S. *Appl. Catal., A* **1997**, *163*, 261−273.
(19) Liu, Z.; Ji, W.; Dong, L.; Chen, Y. *J. Solid State Chem.* **1998**, *138*, 41−46.
(20) Garvie, R. C. *J. Phys. Chem.* **1965**, *69*, 1238−1243.
(21) Wang, H.; Li, G.; Xue, Y.; Li, L. *J. Solid State Chem.* **2007**, *180*, 2790−2797.
(22) Li, W.; Huang, H.; Li, H.; Zhang, W.; Liu, H. *Langmuir* **2008**, *24*, 8358−8366.
(23) Reidy, C. J.; Fleming, T. J.; Hampshire, S.; Towler, M. R. *Int. J. Appl. Ceram. Technol.* **2011**, *8*, 1475−1485.
(24) Bellido, J. D. A.; De Souza, J. E.; M'Peko, J.-C.; Assaf, E. M. *Appl. Catal., A* **2009**, *358*, 215−223.
(25) Tani, E.; Yoshimura, M.; SŌMiya, S. *J. Am. Ceram. Soc.* **1983**, *66*, 11−14.
(26) Noh, H.-J.; Seo, D.-S.; Kim, H.; Lee, J.-K. *Mater. Lett.* **2003**, *57*, 2425−2431.
(27) Song, Y.-Q.; Liu, H.-M.; He, D.-H. *Energy Fuels* **2010**, *24*, 2817−2824.
(28) Elam, J. W.; Groner, M. D.; George, S. M. *Rev. Sci. Instrum.* **2002**, *73*, 2981−2987.
(29) Christensen, S. T.; Elam, J. W.; Rabuffetti, F. A.; Ma, Q.; Weigand, S. J.; Lee, B.; Seifert, S.; Stair, P. C.; Poeppelmeier, K. R.; Hersam, M. C.; Bedzyk, M. J. *Small* **2009**, *5*, 750−757.
(30) Jung, K. T.; Bell, A. T. *J. Mol. Catal A: Chem.* **2000**, *163*, 27−42.
(31) Bollmann, L.; Ratts, J. L.; Joshi, A. M.; Williams, W. D.; Pazmino, J.; Joshi, Y. V.; Miller, J. T.; Kropf, A. J.; Delgass, W. N.; Ribeiro, F. H. *J. Catal.* **2008**, *257*, 43−54.
(32) Williams, W. D.; Shekhar, M.; Lee, W.-S.; Kispersky, V.; Delgass, W. N.; Ribeiro, F. H.; Kim, S. M.; Stach, E. A.; Miller, J. T.; Allard, L. F. *J. Am. Chem. Soc.* **2010**, *132*, 14018−14020.
(33) Shekhar, M.; Wang, J.; Lee, W.-S.; Williams, W. D.; Kim, S. M.; Stach, E. A.; Miller, J. T.; Delgass, W. N.; Ribeiro, F. H. *J. Am. Chem. Soc.* **2012**, *134*, 4700−4708.
(34) Mamott, G. T.; Barnes, P.; Tarling, S. E.; Jones, S. L.; Norman, C. J. *J. Mater. Sci.* **1991**, *26*, 4054−4061.
(35) Dell'Agli, G.; Colantuono, A.; Mascolo, G. *Solid State Ionics* **1999**, *123*, 87−94.
(36) Rabuffetti, F. A.; Kim, H.-S.; Enterkin, J. A.; Wang, Y.; Lanier, C. H.; Marks, L. D.; Poeppelmeier, K. R.; Stair, P. C. *Chem. Mater.* **2008**, *20*, 5628−5635.
(37) Xu, X.; Wang, X. *Nano Res.* **2009**, *2*, 891−902.
(38) Jiao, X.; Chen, D.; Xiao, L. *J. Cryst. Growth* **2003**, *258*, 158−162.
(39) Stefanic, G.; Music, S. *Croat. Chem. Acta* **2002**, *75*, 727−767.
(40) Ho, S. M. *Mater. Sci. Eng.* **1982**, *54*, 23−29.
(41) Wagner, C. D.; Zatko, D. A.; Raymond, R. H. *Anal. Chem.* **1980**, *52*, 1445−1451.
(42) Allen, G. C.; Curtis, M. T.; Hooper, A. J.; Tucker, P. M. *J. Chem. Soc., Dalton Trans.* **1974**, 1525−1530.
(43) Bartholomew, C. H.; Farrauto, R. J. *Fundamentals of Industrial Catalytic Processes*, 2nd ed.; John Wiley & Sons, Inc.: Hoboken, NJ, 2005.
(44) Panagiotopoulou, P.; Kondarides, D. I. *Catal. Today* **2006**, *112*, 49−52.
(45) Pazmino, J. H.; Shekhar, M.; Damion Williams, W.; Cem Akatay, M.; Miller, J. T.; Nicholas Delgass, W.; Ribeiro, F. H. *J. Catal.* **2012**, *286*, 279−286.
(46) Zhai, Y.; Pierre, D.; Si, R.; Deng, W.; Ferrin, P.; Nilekar, A. U.; Peng, G.; Herron, J. A.; Bell, D. C.; Saltsburg, H.; Mavrikakis, M.; Flytzani-Stephanopoulos, M. *Science (Washington, DC, U. S.)* **2010**, *329*, 1633−1636.
(47) Zhu, X.; Shen, M.; Lobban, L. L.; Mallinson, R. G. *J. Catal.* **2011**, *278*, 123−132.